Strain effects on the magnon-magnon interaction and magnon relaxation time in ferromagnetic $CrGeTe_3$

Ke Wang,[1,*] Kai Ren,[2] Yinlong Hou,[1] Dan Yang,[1] and Gang Zhang[3,†]

[1] *School of automation, Xi'an University of Posts & Telecommunications, Shaanxi, 710121, China*

[2] *School of Mechanical and Electronic Engineering, Nanjing Forestry University, Nanjing, Jiangsu 210042, China*

[3] *Yangtze Delta Region Academy of Beijing Institute of Technology (Jiaxing), Jiaxing, Zhejiang 314019, China*

(Received 22 January 2024; revised 24 March 2024; accepted 29 April 2024; published 20 May 2024)

In the synthesis of two-dimensional (2D) materials and the fabrication of 2D devices, the strain introduced by lattice mismatch is inevitable. Meanwhile, strain is also a frequently used strategy to improve the Curie temperature of 2D magnets. However, the impact of strain on the magnon relaxation time is unclear. In this work, we investigated the impacts of strain on the magnon-magnon interaction and magnon relaxation time in the ferromagnetic $CrGeTe_3$ monolayer by combining first-principles calculations and theoretical analysis. We find the magnon relaxation times in strained and unstrained $CrGeTe_3$ monolayers have similar dependences on temperature, wave vectors, and magnetic fields. However, the magnon relaxation time is remarkably reduced by tensile strain. When the external magnetic field is 0.1 T, the maximum shortened ratio of the magnon relaxation time can reach 49.3%, revealing an enhancement of the magnon-magnon interaction. With the magnetic field strengthening, the shortened ratio of the magnon relaxation time decreases, but it still reaches up to 19.4% under a 5-T magnetic field. This shortening of magnon relaxation time is undesired for applications in spintronics. Our work provides physical insights into the impacts of strain on 2D magnets.

DOI: 10.1103/PhysRevApplied.21.054036

I. INTRODUCTION

In the past two decades, two-dimensional (2D) materials have been widely applied in various fields, including electronics [1,2], energy [3,4], and biomedicine [5,6]. The 2D magnet is an important member of the family of 2D materials. Compared to nonmagnetic 2D materials, 2D magnets can be applied in data storage [7,8], signal transfer [9,10], and spincaloritronics [11,12], due to their controllable magnetoresistance [13], large spin Seebeck coefficients [14], and the quantized anomalous Hall effect [15]. In magnetic materials, the quantization of the spin wave is defined as a magnon. In signal transfer using spin as a carrier, the transmission distance is strongly related to the magnon lifetime, and a long magnon lifetime is preferred [16,17]. In 2D magnets, the magnon lifetime is determined by the magnon-phonon, magnon-magnon, and magnon-carrier interactions. In recent years, Wang *et al.* studied the magnon lifetime governed by the magnon-phonon interaction in 2D magnets [18,19]. It was found that the acoustic and optical magnon lifetimes governed by the magnon-phonon interaction showed linear and quadratic dependences on the wave vector, respectively, and the magnon lifetime governed by the magnon-phonon interaction depended heavily on the temperature. In 2017, few-layer ferromagnetic CrI_3 [20] and $CrGeTe_3$ [21] were synthesized successfully by mechanical exfoliation. Subsequently, various 2D magnets were unveiled and studied, such as ferromagnetic Fe_5GeTe_2 [22], antiferromagnetic $MnPS_3$ [23], conductive Fe_3GeTe_2 [24], room-temperature magnetic $CrTe_2$ [25], and $MnBi_2Te_4$ with the quantized anomalous Hall effect [26,27].

In practical applications, the spintronics device performance is strongly dependent on the quality of 2D magnetic materials. Thus, the controllable synthesis of 2D magnetic materials with high quality is essential for their large-scale applications. Mechanical exfoliation and chemical vapor deposition are two frequently used synthesis methods for 2D magnetic materials [28,29]. Furthermore, the synthesized 2D magnets need to be transferred to the SiO_2/Si substrate for the detection of magnetic orders and the measurement of physical properties in experiments. During both the mechanical exfoliation and transfer processes, it is inevitable that strain is introduced into 2D magnets, due to the lattice mismatch between 2D magnets and the substrate. Meanwhile, strain is also an effective and frequently used strategy to tailor the physical and chemical properties of 2D materials. Thus, several researchers have investigated the influences of strain on the electronic, phononic, and thermal properties of 2D magnetic materials [30–34], which can provide theoretical guidance and support for

*Corresponding author: kewang@xupt.edu.cn

†Corresponding author: gangzhang2006@gmail.com

the manufacturing of nanosized spintronic devices. For instance, Liu *et al*. [35] improved the strength of magnetic exchange coupling and the Curie temperature of $CrGeTe_3$ significantly by the biaxial in-plane strain, while Webster and Yan [36] manipulated the magnetic phase between ferromagnetism and antiferromagnetism, as well as the out-of-plane magnetic anisotropy energy of the CrI_3 monolayer by in-plane biaxial strain. However, the impact of strain on the magnon lifetime is still unclear, which is adverse for the applications of 2D magnets in information technology.

In this paper, we took the $CrGeTe_3$ monolayer as an example to explore the effect of strain on the magnon lifetime dominated by the magnon-magnon interaction. Because the $CrGeTe_3$ monolayer is a magnetic semiconductor with an indirect band gap, it has an ultralow carrier concentration near the Fermi level and a weak magnon-carrier interaction. Additionally, the appearance of out-of-plane magnetic anisotropy in 2D magnets increases the difficulty of theoretical studies and analysis for magnon lifetimes. In the CrI_3 monolayer, the magnetic anisotropy is remarkable and up to about 29.3% of the nearest-neighbor magnetic exchange constant [37]. Unlike CrI_3, the magnetic anisotropy in the $CrGeTe_3$ monolayer is only 2% of the magnetic exchange constant and can be ignored [38,39], which simplifies the calculation of magnon lifetime and has little effect on the Curie temperature of the $CrGeTe_3$ monolayer [40–42]. Here, we combined first-principles calculations and theoretical analysis to obtain the magnon lifetime governed by the magnon-magnon interaction in strained and unstrained $CrGeTe_3$ monolayers, for a comprehensive insight into the effect of strain on magnon-magnon interactions and the magnon relaxation time. We find that, although strain has little influence on the dependence of the magnon relaxation time with temperature, wave vector, and external magnetic field, strain can reduce the magnon relaxation time significantly. These findings are of significance for designing 2D electromechanical devices, spintronics devices, and nanosized strain sensors.

II. METHODS

A. Computational details

In this work, the Vienna *ab initio* simulation package [43,44] was used to implement all first-principles calculations with the exchange-correlation functional of the Perdew-Burke-Ernzerhof method of the generalized gradient approximation [45,46]. Meanwhile, the GGA + U approach introduced by Dudarev *et al*. [47] was used to describe the d-orbital electrons in Cr^{3+} ions, and the effective Hubbard "$U_{\text{eff}} = U$-J" was set as 1 eV, as used previously in the literature [38,48]. We select this value because Gong *et al*. [21] and Kang *et al.* [49] reported that the value of "U_{eff}" for the Cr^{3+} ions in $CrGeTe_3$ should be between 0.2 and 1.7 eV; otherwise, the calculated band gap and magnetic ground state may be contrary to the experimental results. In establishing the 2D model of the $CrGeTe_3$ monolayer, we imposed a 20-Å vacuum space along the c axis to weaken the possible interaction between adjacent layers. In the optimization of the geometrical structure, the $CrGeTe_3$ monolayer was relaxed with the 500-eV cutoff energy and the $5 \times 5 \times 1$ [(MP) Monkhorst-Pack] grid until the energy and atom force converged to 10^{-8} eV and 0.001 eV/Å, respectively. In self-consistent calculations, a denser MP grid of $9 \times 9 \times 1$ was set to calculate the energy difference between possible magnetic configurations. Monte Carlo simulations based on the Heisenberg model were implemented by the MCSOLVER code to obtain the Curie temperature of the $CrGeTe_3$ monolayer with and without strain [50,51], which was commonly used in previous studies [52–54]. Besides, the density-functional perturbation theory was used to calculate phonon dispersions [55], as implemented by the PHONOPY code.

B. Magnon dispersion and spin autocorrelation function at finite temperature

Before discussing magnon dispersion and magnon-magnon interactions, it is necessary to determine the magnetic ground state of 2D magnets. The diagram of four possible magnetic configurations is presented in Fig. S1 within the Supplemental Material [56]. For the $CrGeTe_3$ monolayer, the total energies of Néel-, stripy-, and zigzag-antiferromagnetic (AFM) configurations are 93.22, 54.54, and 31.24 meV per unit cell higher than the ferromagnetic (FM) phase, respectively. Therefore, the magnetic ground state of the $CrGeTe_3$ monolayer is ferromagnetic and can be identified by the spin-density distribution in Fig. S1(b) within the Supplemental Material [56]. Meanwhile, these energy difference between Néel-, stripy-, and zigzag-AFM and FM states can also be used to calculate the magnetic exchange constants [57,58]. Due to the small second-nearest- and third-nearest-neighbor magnetic exchange constants in the $CrGeTe_3$ monolayer, we only consider the contribution of nearest-neighbor magnetic exchange coupling (J_1) in this paper. The value of J_1 can be obtained from Eq. (S7) within the Supplemental Material [56], which is strongly related to the distance between two magnetic sites [59,60]. Therefore, strain can tailor the value of J_1 effectively.

After obtaining the magnetic exchange constant, the magnon dispersion can be calculated by diagonalizing the Hamiltonian. In 2020, Wang *et al*. [61] calculated the magnon dispersion at finite temperature by

$$\hbar\omega_k^{\pm}(T) = 3J_1S_0(1 \pm \gamma_k) - 3J_1S_0(1 \pm \gamma_k) \times \frac{1}{NS_0}\sum_{k'}(1 - \gamma_{k'})\left\langle a_{k'}^{+}a_{k'}\right\rangle_T + 2g\mu_B B, \quad (1)$$

with $\gamma_k = 1/3 \sum_{i,j \in N} e^{ik(r_j - r_i)}$. ω^+ and ω^- represent the magnon frequencies for optical and acoustic magnon branches, respectively. Details of Eq. (1) can be found in Part 2 and Part 3 of Ref. [56]. In the derivation, the Holstein-Primakoff approximation [62,63] and Wick theory [64] were used. Furthermore, the contribution from the temperature-dependent magnon operators, dominated by the "dynamical magnon-magnon interaction," was considered, due to the failure of the low-temperature approximation at nonzero temperature [65,66]. This contribution can be gained by a self-consistent procedure with a convergence limit of 10^{-5} eV. The first term is the static magnon energy without temperature dependence, while the last term is the Zeeman term induced by an external magnetic field. In this work, we also use this method to calculate the magnon dispersions at finite temperatures for pristine and strained $CrGeTe_3$ monolayers. It is worth emphasizing that the magnetic exchange constant, J_1, of the $CrGeTe_3$ monolayer is insensitive to the increase of temperature [18]. Thus, in this work, we neglect the temperature dependence of J_1 and only consider the magnon redistribution induced by finite temperature to calculate the magnon dispersion.

III. RESULTS AND DISCUSSION

A. Stability of pristine and strained $CrGeTe_3$ monolayers

The lattice parameters of the optimized $CrGeTe_3$ monolayer are $a = b = 6.91$ Å, which are slightly larger than the experimental values ($a = b = 6.83$ Å) but consistent with previous theoretical studies [38,67,68]. The top and side views of the optimized $CrGeTe_3$ monolayer are presented in Fig. 1(a), where each Cr and Ge atom is surrounded by six Te atoms. The high-symmetry path in the irreducible Brillouin zone of the $CrGeTe_3$ monolayer is shown in Fig. 1(b), which is used in plotting the phonon and magnon dispersions. Here, the phonon dispersion was calculated to identify the thermodynamic stability of our optimized $CrGeTe_3$ monolayer, and the calculated phonon dispersion is presented in Fig. S2(a) within the Supplemental Material [56]. There is no obvious imaginary frequency in the phonon dispersion, indicating the thermodynamic stability of the optimized $CrGeTe_3$ monolayer. Besides, we also calculated the stiffness tensor of the optimized $CrGeTe_3$ monolayer, as shown in Table S1 within the Supplemental Material [56]. In Table S1 within the Supplemental Material [56], we find that the values of C11, C12, and C66 are 56.098, 56.098, and 22.425 N/m, respectively, and all of them satisfy the Born-Huang stability criteria [69], revealing the mechanical stability of the optimized $CrGeTe_3$ monolayer. The stress-strain relationship of the optimized $CrGeTe_3$ monolayer was calculated by using the strain-energy method [70], as presented in Fig. S3 within the Supplemental Material [56]. In Fig. S3 within the Supplemental Material [56], it is found that the maximum stress and strain that the optimized $CrGeTe_3$ monolayer can withstand are 20.6 GPa and 21%, respectively. In this paper, the maximum biaxial strain applied to the $CrGeTe_3$ monolayer is 10%. In 2020, Yin *et al.* [71] disclosed the impressive impact of strain on the phononic properties and thermal conductivity of graphenelike borophene, which may destroy the stability of 2D materials. Here, we also calculated the phonon dispersion of the 10% strained $CrGeTe_3$ monolayer, as shown in Fig. S2(b) within the Supplemental Material [56]. It is noted that, although strain decreases the highest phonon frequency significantly, there is still no obvious imaginary frequency, indicating the thermodynamics of the 10% strained $CrGeTe_3$ monolayer.

B. Magnon dispersion of pristine and strained $CrGeTe_3$

After structural optimization, we implemented self-consistent calculations of the FM and AFM configurations to obtain the magnetic exchange constants of pristine and

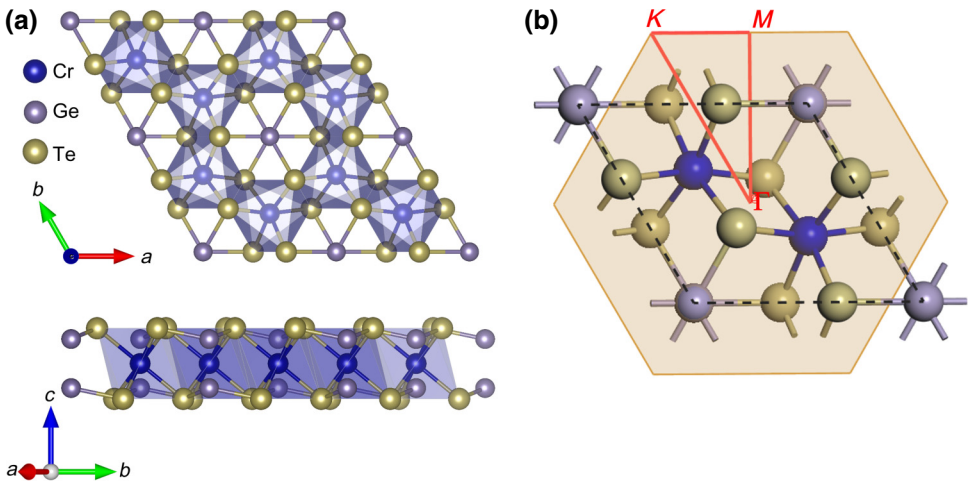

FIG. 1. Geometrical structure (a) and high-symmetry path in the irreducible Brillouin zone (b) of the $CrGeTe_3$ monolayer.

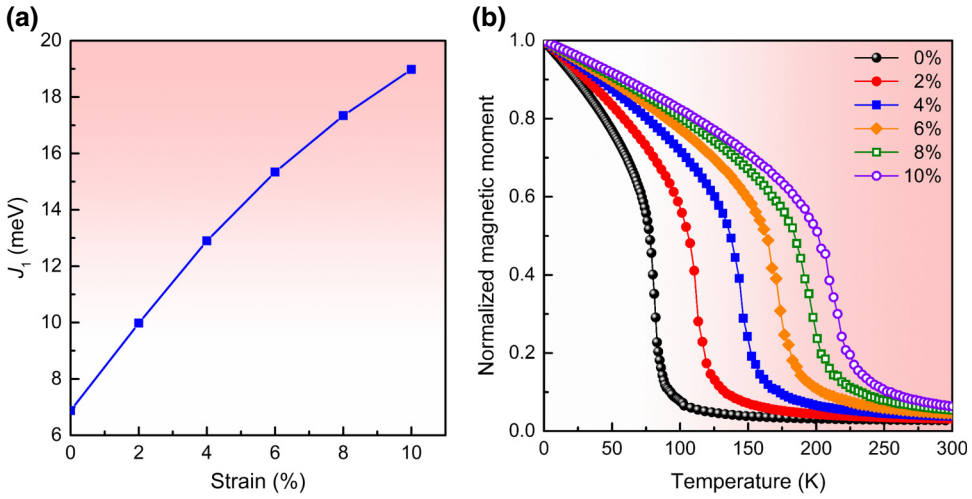

FIG. 2. Magnetic exchange constant (a) and Curie temperature (b) of pristine and strained $CrGeTe_3$ monolayers.

strained $CrGeTe_3$ monolayers from Eq. (7). The results are shown in Fig. 2(a). It can be found that the magnetic exchange constant increases with biaxial tensile strain monotonously, and the enhancement can be up to about 176%, which is in agreement with the enhancement of 191% reported in Ref. [35]. Based on these magnetic exchange constants and the Heisenberg model, we employed Monte Carlo simulations and calculated the temperature dependence of the magnetic moment, as shown in Fig. 2(b). The Curie temperature is elevated from 85 to 215 K, corresponding to an enhancement ratio of about 153%. These results suggest that tensile strain is an effective strategy to improve the low Curie temperature of 2D magnets and promote their application in spintronics. In the $CrGeTe_3$ monolayer, the strength of magnetic exchange coupling is dominated by the competition between AFM direct- and FM superexchange couplings [72,73]. The AFM direct-exchange coupling depends heavily on the distance between two magnetic Cr^{3+} ions in the $CrGeTe_3$ monolayer. According to the Goodenough-Kanamori rule [74,75], the superexchange coupling depends strongly on the Cr-Te-Cr angle. Once tensile strain is applied, the distance between two magnetic atoms increases significantly from 3.94 Å (pristine) to 4.34 Å (10% strain), suppressing the AFM direct-exchange coupling. Meantime, the Cr-Te-Cr angle changes slightly. Hence, the difference between FM super- and AFM direct-exchange couplings increases with tensile strain, and the magnetic exchange constant is enhanced by strain remarkably.

Subsequently, the obtained magnetic exchange constants were substituted into Eq. (12), and then the magnon dispersions, considering the contribution from dynamic magnon-magnon interactions, were calculated, as shown in Fig. 3. In Eq. (12), there are two factors affecting the magnon frequency: the temperature (T) and the external magnetic field (B). In Figs. 3(a) and 3(b), we plot the magnon dispersions of pristine $CrGeTe_3$ monolayers at finite temperatures and different external magnetic fields, where the insets are the enlarged dispersion curves near the center point (Γ point) of the irreducible Brillouin zone. Interestingly, the external magnetic field can open a gap between the acoustic branch and zero frequency at the Γ point, and the gap becomes large as the external magnetic field increases, as shown in the inset of Fig. 3(b) (in the purple rectangle). Meantime, we find that the magnon frequency also increases with the external magnetic field but decreases with temperature, as shown in the insets of Figs. 3(a) and 3(b) (in the green rectangle). To highlight the temperature dependence of magnon frequency, we analyze the changes to acoustic and optical magnon frequencies with temperature at several wave vectors, as shown in Fig. S4 within the Supplemental Material [56]. Obviously, all magnon frequencies reduce with temperature monotonously, and the reduction of the optical magnon is more remarkable than that of the acoustic magnon. These results reveal that the contribution of dynamic magnon-magnon interactions is to decrease the magnon frequency, and this reduction is positively correlated with the static magnon energy. This finding is consistent with the results and physical model reported in Ref. [76].

In Fig. 3(c), the magnon dispersions of the strained $CrGeTe_3$ monolayer are presented. It is clear that the frequency of the optical magnon increases with tensile strain significantly; this is caused by the enhancement of the magnetic exchange constant. To observe the influence of strain on the magnon frequency quantitatively, we plot the temperature-dependent magnon frequencies of acoustic and optical magnons of the strained $CrGeTe_3$ monolayer in Fig. 4. For the 4% strained $CrGeTe_3$ monolayer,

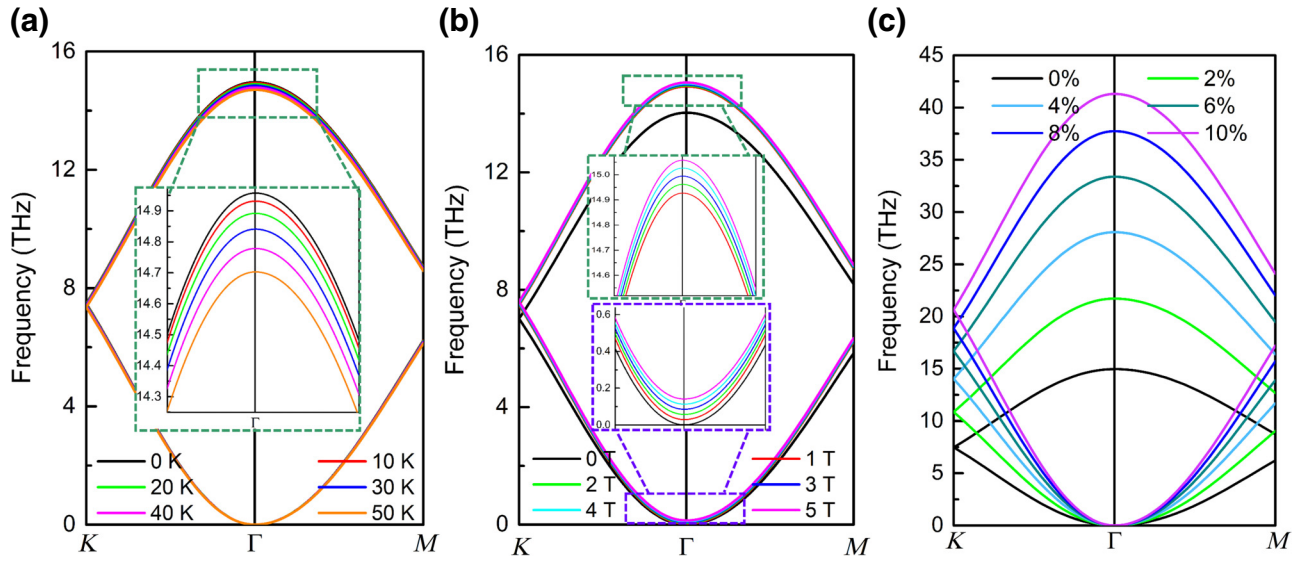

FIG. 3. Magnon dispersions of the pristine $CrGeTe_3$ monolayer at different temperatures (a) and external magnetic fields (b), and magnon dispersion of the strained $CrGeTe_3$ monolayer (c). Insets in (a),(b) are enlarged dispersion curves near the center point of the irreducible Brillouin zone.

all frequencies of the acoustic and optical magnons at wave vectors (k) of 9.0×10^5 cm^{-1} ($0.02\pi/a$), 4.5×10^6 cm^{-1} ($0.10\pi/a$), 1.35×10^7 cm^{-1} ($0.30\pi/a$), 2.25×10^7 cm^{-1} ($0.50\pi/a$), 3.15×10^7 cm^{-1} ($0.70\pi/a$), and 4.5×10^7 cm^{-1} ($1.0\pi/a$) decrease with temperature, as shown in Figs. 4(a) and 4(b). Meanwhile, the decrease relies on the static magnon energy, which agrees well with that in the pristine $CrGeTe_3$ monolayer. However, for strained $CrGeTe_3$ monolayers, the decrease in magnon frequency induced by finite temperature is smaller than that of the pristine $CrGeTe_3$ monolayer, as shown in Fig. 4(c). The reason is that tensile strain enhances the strength of magnetic exchange coupling and elevates the magnon frequency significantly. Therefore, the magnons become difficult to excite.

C. Magnon relaxation time of pristine and strained $CrGeTe_3$

To evaluate the strength of the dynamic magnon-magnon interaction and the effects of strain on the magnon-magnon interaction, the spin autocorrelation functions [$\langle S_k^+(t)S_{-k}^-(0)\rangle$, $\langle S_k^-(t)S_{-k}^+(0)\rangle$, and $\langle S_k^z(t)S_{-k}^z(0)\rangle$] were employed. In this paper, the external magnetic field is applied along the z axis, so $\langle S_k^z(t)S_{-k}^z(0)\rangle$ is particularly emphasized:

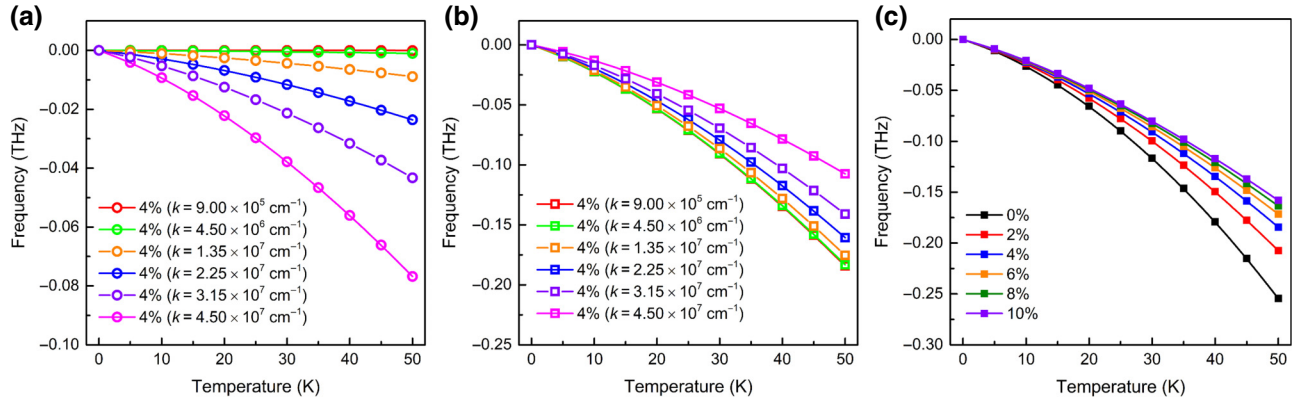

FIG. 4. Sampled contribution of dynamic magnon-magnon coupling for the acoustic (a) and optical (b) magnon frequencies of 4% strained $CrGeTe_3$ monolayer, and (c) temperature dependence of optical magnon frequencies at the Γ point of strained $CrGeTe_3$ monolayers.

$$\left\langle S_k^z(t)S_{-k}^z(0)\right\rangle = \frac{\mathrm{Tr}\left\{e^{-\theta H}\left(\left(N^{1/2}S_0\delta_{k,0} - N^{-1/2}\sum_{k'} a_{k'}^{+}(t)a_{k'+k}(t)\right)\left(N^{1/2}S_0\delta_{-k,0} - N^{-1/2}\sum_{k''} a_{k''}^{+}(0)a_{k''-k}(0)\right)\right)\right\}}{\mathrm{Tr}\{e^{-\theta H}\}},$$

$$= NS_0{}^2\delta_{k,0} - 2S_0\delta_{k,0}\sum_{k'}\left\langle a_{k'}^{+}(0)a_{k'+k}(0)\right\rangle + N^{-1}\sum_{k'} e^{-i(\omega_{k'+k}-\omega_{k'})t}\left\langle a_{k'}^{+}(0)a_{k'+k}(0)a_{k'+k}^{+}(0)a_{k'}(0)\right\rangle. \quad (2)$$

Obviously, there is a four-magnon term, which is difficult to solve numerically. In Ref. [61], Wick's theorem was employed to decouple the four-magnon term into numerous two-magnon terms, and then $\left\langle S_k^z(t)S_{-k}^z(0)\right\rangle$ could be rewritten as follows:

$$\left\langle S_k^z(t)S_{-k}^z(0)\right\rangle = \begin{cases} NS_0{}^2\delta_{k,0} - 2S_0\delta_{k,0}\sum_{k'}\left\langle a_{k'}^{+}a_{k'}\right\rangle + N^{-1}\sum_{k'}\left(2\left\langle a_{k'}^{+}a_{k'}\right\rangle^2 + \left\langle a_{k'}^{+}a_{k'}\right\rangle\right) & (k=0), \\ N^{-1}\sum_{k'} e^{-\mathrm{i}(\omega_{k'+k}-\omega_{k'})t}\left\langle a_{k'}^{+}a_{k'}\right\rangle\left\langle a_{k'+k}^{+}a_{k'+k}+1\right\rangle & (k\neq 0). \end{cases} \quad (3)$$

First, we calculated the spin autocorrelation functions of the pristine $CrGeTe_3$ monolayer under finite temperature and nonzero external magnetic field at $k = 9.0\times10^5$ cm^{-1} ($0.02\pi/a$), as shown in Fig. S5 within the Supplemental Material [56]. It can be observed that the amplitude of $\left\langle S_k^z(0)S_{-k}^z(0)\right\rangle$ grows with temperature but decreases with the magnetic field, because the amplitude of $\left\langle S_k^z(0)S_{-k}^z(0)\right\rangle$ in Eq. (3) is determined by the magnon density $\left\langle a_k^{+}a_k\right\rangle$. As the temperature increases, more magnons are excited, and the value of $\left\langle a_k^{+}a_k\right\rangle$

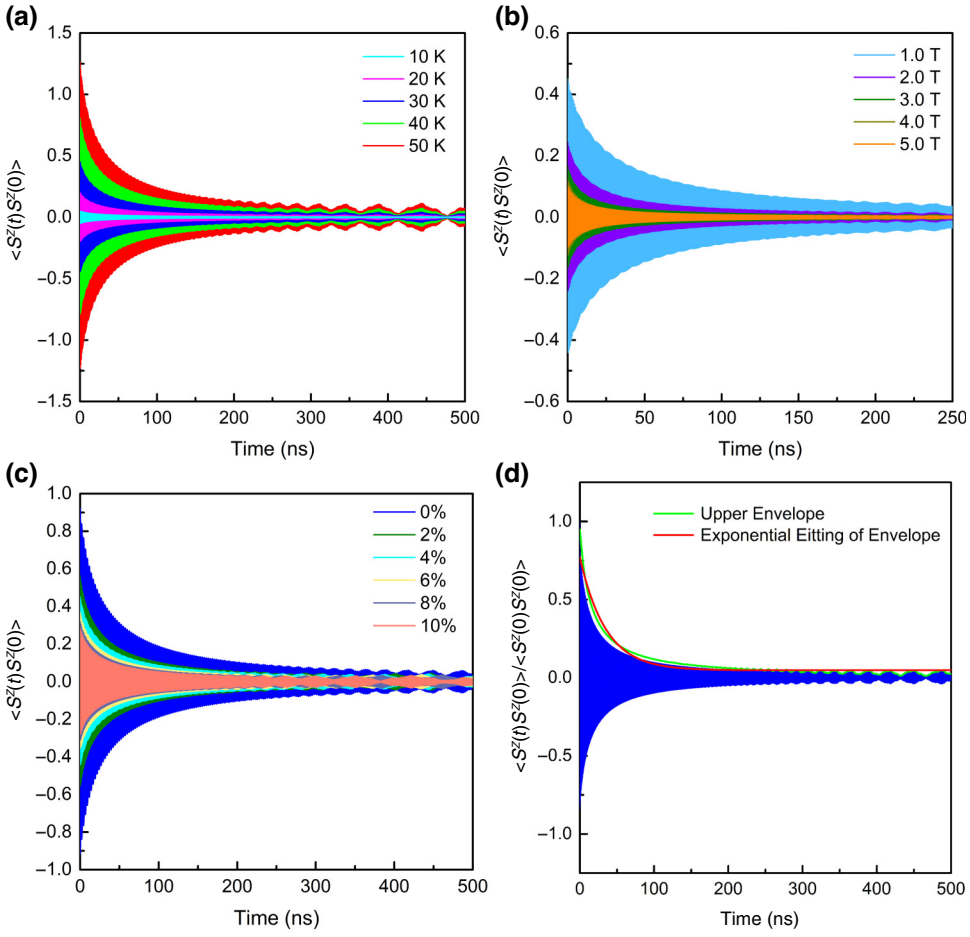

FIG. 5. Spin autocorrelation functions of 4% strained $CrGeTe_3$ monolayer at $k = 9.0\times10^5$ cm^{-1} ($0.02\pi/a$) under different temperatures (T) (a) and external magnetic fields (B) (b), spin autocorrelation functions of unstrained and strained $CrGeTe_3$ monolayers at $k = 0.02\pi/a$ under $T = 30$ K and $B = 1$ T (c), and the diagram of normalized spin autocorrelation function (d).

increases. Meanwhile, a stronger external magnetic field results in higher magnon frequencies and leads to a reduction of the excited magnon density. To identify this analysis, we present the magnetic moment per Cr^{3+} ion $\left[M(B,T) = M_0\left(1 - (1/NS_0)\sum_k \langle a_k^+ a_k\rangle_{B,T}\right)\right]$ versus magnetic field in the pristine $CrGeTe_3$ monolayer in Fig. S6 within the Supplemental Material [56], where the temperature grows from 0 to 50 K. In Fig. S6 within the Supplemental Material [56], the magnetic moment increases with strengthening of the magnetic field and tends to a specific value, but it is reduced close to zero as the temperature increases. These results are consistent with our analysis of the influences of temperature and external magnetic field on the magnon density $\langle a_k^+ a_k\rangle$. Similar phenomena can also be found in the 4% strained $CrGeTe_3$ monolayer, as shown in Figs. 5(a), 5(b), and 6(a).

In Fig. 5(c), the spin autocorrelation functions of unstrained and strained $CrGeTe_3$ monolayers at $k = 0.02\pi/a$ at 30 K and under a magnetic field of 1 T are presented. Obviously, the amplitude of $\langle S_k^z(0)S_{-k}^z(0)\rangle$ decreases with the applied strain monotonically. This is due to the enhancement of magnetic exchange coupling and magnon frequency by strain, as shown in Figs. 2(a) and 3(c). The enhancement of the magnon frequency makes the excitation of magnons difficult, and then the magnon density $\langle a_k^+ a_k\rangle$ is reduced at a wave vector of $0.02\pi/a$. The magnetic moments per Cr^{3+} ion in unstrained and strained $CrGeTe_3$ monolayers versus the external magnetic field are shown in Fig. 6(b), where the temperature is set to 30 K. In Fig. 6(b), we find that the magnetic moment increases with the applied strain at a specific magnetic field, suggesting a reduction of the magnon density with strain. This agrees with the results in Figs. 4(c) and 5(c).

We extracted the magnon relaxation time by fitting the upper envelope of the normalized spin autocorrelation function exponentially with a decay function $[f(t) = A\exp(-t/\tau_{MM})]$, as shown in Fig. 5(d). The blue, green, and red lines represent the normalized spin autocorrelation function, the upper envelope, and the exponential fitting of the upper envelope, respectively. The relaxation time, τ_{MM}, of the spin autocorrelation function can reflect the strength of the magnon-magnon interaction, and a shorter τ_{MM} corresponds to a stronger magnon-magnon interaction. The extracted magnon relaxation times of pristine and strained $CrGeTe_3$ monolayers are presented in Fig. 7. In Fig. 7(a), the magnon relaxation times of both pristine and strained $CrGeTe_3$ monolayers are significantly reduced with an increase of the wave vector from $0.02\pi/a$ to $0.3\pi/a$, and then gradually decrease with the wave vector, when the temperature and external magnetic field are 30 K and 1 T, respectively. Furthermore, strain has little effect on this downward trend, and only decreases the magnon relaxation time. The maximum shortened ratio induced by 10% strain is about 51.22% at $k = 0.2\pi/a$,

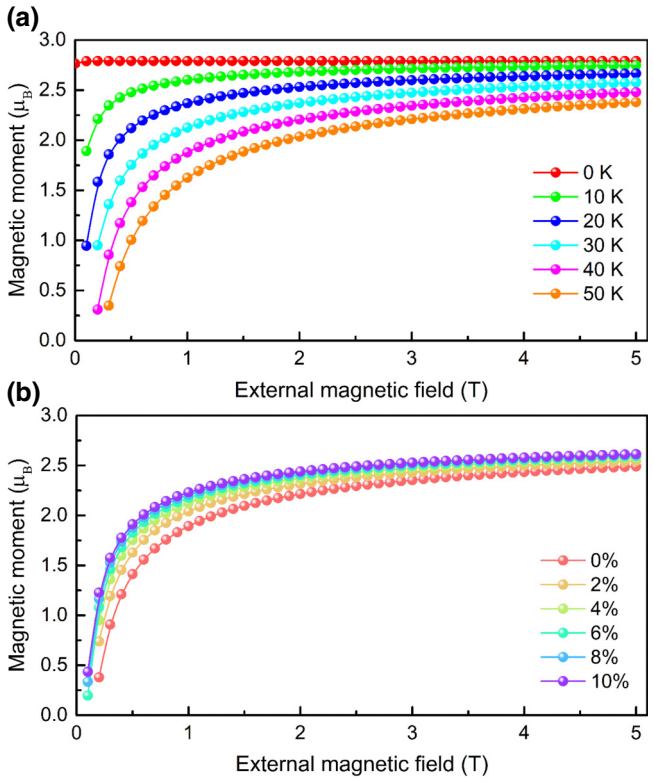

FIG. 6. (a) Magnetic moment per Cr^{3+} ion in 4% strained $CrGeTe_3$ monolayer versus magnetic field. In (a), the temperature changes from 0 to 50 K. (b) Magnetic moment per Cr^{3+} ion in unstrained and strained $CrGeTe_3$ monolayers versus magnetic field at 30 K.

revealing the remarkable enhancement of the magnon-magnon interaction by strain. At $k = 0.02\pi/a$, the shortened ratio induced by 10% strain is also up to about 13.3%. In Fig. 7(b), the magnon relaxation times of both pristine and strained $CrGeTe_3$ monolayers are reduced significantly with temperature from 1 to 10 K, and then change slightly as the temperature increases from 10 to 55 K, when the wave vector and the external magnetic field are $0.02\pi/a$ and 1 T, respectively. This trend is also not affected by strain. When the temperature is close to 0 K, the shortened ratio induced by 10% strain is 8.3%, while it is around 13% as the temperature increases.

As shown in Fig. 7(c), the magnon relaxation times of both pristine and strained $CrGeTe_3$ monolayers are reduced continuously as the external magnetic field increases from 0.1 to 5 T, when the wave vector and temperature are $0.02\pi/a$ and 30 K, respectively. Meanwhile, the application of strain also reduces the magnon relaxation time, and the maximum shortened ratio of about 49.3% occurs at a strain and magnetic field of 10% and 0.1 T, respectively. As the external magnetic field increases, the shortened ratio decreases, but is still up to 19.4% at 5 T. These results reveal that the dependence of magnon relaxation

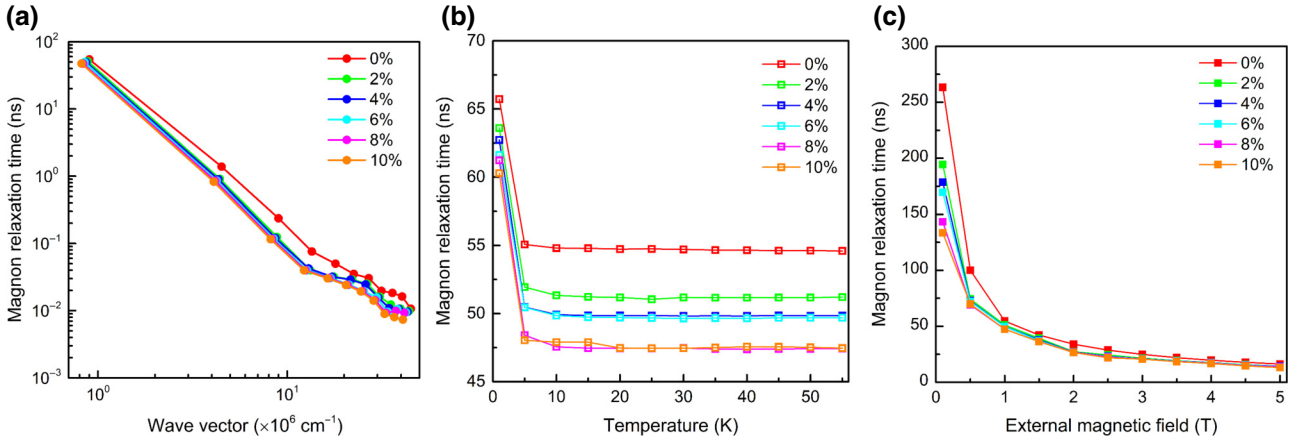

FIG. 7. (a) Dependences of magnon relaxation times in unstrained and strained $CrGeTe_3$ monolayers on wave vector at a temperature of 30 K and external magnetic field of 1 T. (b) Dependences of magnon relaxation times in unstrained and strained $CrGeTe_3$ monolayers on temperature under an external magnetic field of 1 T and wave vector $k = 0.02\pi/a$. (c) Dependences of magnon relaxation times in unstrained and strained $CrGeTe_3$ monolayers on external magnetic field at a temperature of 30 K and wave vector $k = 0.02\pi/a$.

time on wave vector, temperature, and external magnetic field changes slightly with strain, but the value of the magnon relaxation time decreases significantly as the strain increases.

Why does strain suppress the excitation of magnons but reduce the magnon relaxation time? To answer this question, we calculated the values of the magnon group velocity by

$$v_k = \frac{d\omega_k}{dk}. \tag{4}$$

According to Eq. (4), it is clear that the decay rate of the spin autocorrelation function depends on both the magnon density and the frequency difference between the k' and $k' + k$ points, while the frequency difference between the k' and $k' + k$ points near the center of the Brillouin zone can be described by the value of the magnon group velocity. A larger absolute value of group velocity suggests a quicker decay of spin autocorrelation and a shorter magnon relaxation time. The values of magnon group velocity obtained at 30 K are plotted in Fig. 8. At $k = 0.02\pi/a$ (near the center of the Brillouin zone), the enhanced ratios of the magnon group velocity are about 57%, 107%, 152%, 190%, and 223% for 2%, 4%, 6%, 8%, and 10% strained $CrGeTe_3$ monolayers, respectively. Hence, the decay of the spin autocorrelation function quickens with the applied strain, leading to a shortening of the magnon relaxation time, as shown in Fig. 7.

IV. CONCLUSIONS

In this paper, we explored the impact of strain on the magnon relaxation time dominated by magnon-magnon

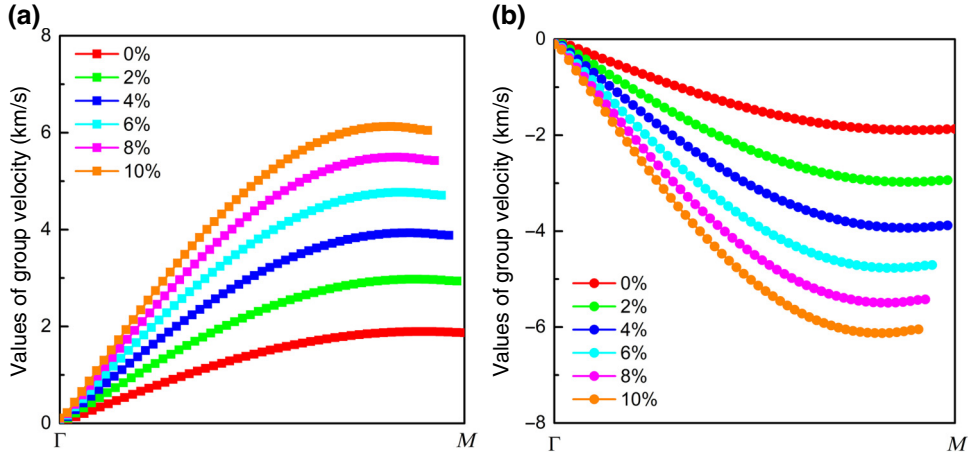

FIG. 8. Values of group velocities for acoustic (a) and optical (b) magnons along the Γ-M path in the irreducible Brillouin zone of unstrained and strained $CrGeTe_3$ monolayers.

interactions in the ferromagnetic $CrGeTe_3$ monolayer by first-principles calculations and theoretical analysis. We find that the in-plane biaxial strain can enhance the magnetic exchange coupling remarkably, improving the Curie temperature of 2D $CrGeTe_3$. The enhancements of the magnetic exchange constant and Curie temperature are up to 176% and 153%, respectively. Meanwhile, the applied strain decreases the magnon relaxation time significantly. At a low magnetic field, the maximum shortened ratio of the magnon relaxation time at $k = 0.02\pi/a$ can reach 49.3%. To elucidate this shortening of the magnon relaxation time induced by strain, we calculated the magnon group velocity and observed that the applied strain could enhance the magnon group velocity significantly. The enhancements of the value of magnon group velocity are about 57%, 107%, 152%, 190%, and 223% for 2%, 4%, 6%, 8%, and 10% strained $CrGeTe_3$ monolayers, respectively, resulting in rapid decay of the spin autocorrelation function and a shortening of the magnon relaxation time.

ACKNOWLEDGMENTS

K.W. acknowledges support from the National Natural Science Foundation of China (NNSFC, Grant No. 12204373), the Shaanxi Provincial Science and Technology Department project (Grant No. 2022JQ-015), and the Shaanxi Association for Science and Technology (Grant No. 20230508). K.R. acknowledges support from the Jiangsu Natural Science Foundation (Grant No. BK20220407). D.Y. acknowledges support from the Shaanxi Provincial Department of Education Project (Grant No. 23JK0677).

The authors declare no competing financial interest.

[1] N. R. Glavin, R. Rao, V. Varshney, E. Bianco, A. Apte, A. Roy, E. Ringe, and P. M. Ajayan, Emerging applications of elemental 2D materials, Adv. Mater. **32**, 1904302 (2020).

[2] L. Tong, Z. Peng, R. Lin, Z. Li, Y. Wang, X. Huang, K.-H. Xue, H. Xu, F. Liu, H. Xia, *et al.*, 2D materials–based homogeneous transistor-memory architecture for neuromorphic hardware, Science **373**, 1353 (2021).

[3] F. R. Fan, R. Wang, H. Zhang, and W. Wu, Emerging beyond-graphene elemental 2D materials for energy and catalysis applications, Chem. Soc. Rev. **50**, 10983 (2021).

[4] Z. Huo, Y. Wei, Y. Wang, Z. L. Wang, and Q. Sun, Integrated self-powered sensors based on 2D material devices, Adv. Funct. Mater. **32**, 2206900 (2022).

[5] T. Fan, L. Yan, S. He, Q. Hong, F. Ai, S. He, T. Ji, X. Hu, E. Ha, B. Zhang, *et al.*, Biodistribution, degradability and clearance of 2D materials for their biomedical applications, Chem. Soc. Rev. **51**, 7732 (2022).

[6] H. Huang, W. Feng, and Y. Chen, Two-dimensional biomaterials: material science, biological effect and biomedical engineering applications, Chem. Soc. Rev. **50**, 11381 (2021).

[7] F. Xue, C. Zhang, Y. Ma, Y. Wen, X. He, B. Yu, and X. Zhang, Integrated memory devices based on 2D materials, Adv. Mater. **34**, 2201880 (2022).

[8] A. Pal, S. Zhang, T. Chavan, K. Agashiwala, C.-H. Yeh, W. Cao, and K. Banerjee, Quantum-engineered devices based on 2D materials for next-generation information processing and storage, Adv. Mater. **35**, 2109894 (2023).

[9] J. Li, C. B. Wilson, R. Cheng, M. Lohmann, M. Kavand, W. Yuan, M. Aldosary, N. Agladze, P. Wei, M. S. Sherwin, *et al.*, Spin current from sub-terahertz-generated antiferromagnetic magnons, Nature **578**, 70 (2020).

[10] J. C. Slonczewski, Current-driven excitation of magnetic multilayers, J. Magn. Magn. Mater. **159**, L1 (1996).

[11] E. Elahi, G. Dastgeer, G. Nazir, S. Nisar, M. Bashir, H. Akhter Qureshi, D.-k. Kim, J. Aziz, M. Aslam, K. Hussain, *et al.*, A review on two-dimensional (2D) magnetic materials and their potential applications in spintronics and spin-caloritronic, Comp. Mater. Sci. **213**, 111670 (2022).

[12] T. Liu, J. Peiro, D. K. de Wal, J. C. Leutenantsmeyer, M. H. D. Guimarães, and B. J. van Wees, Spin caloritronics in a $CrBr_3$-based magnetic van der Waals heterostructure, Phys. Rev. B **101**, 205407 (2020).

[13] W. Liu, Y. Wang, Y. Han, W. Tong, J. Fan, L. Pi, N. Hao, L. Zhang, and Y. Zhang, Anisotropic magnetoresistance behaviors in the layered ferromagnetic $Cr_2Ge_2Te_6$, J. Phys. D: Appl. Phys. **53**, 025101 (2020).

[14] B. Marfoua, I. Khan, and J. Hong, Giant spin Seebeck effect in two-dimensional ferromagnetic CrI_3 monolayer, Nanotechnology **31**, 455404 (2020).

[15] H. Park, J. Cai, E. Anderson, Y. Zhang, J. Zhu, X. Liu, C. Wang, W. Holtzmann, C. Hu, Z. Liu, *et al.*, Observation of fractionally quantized anomalous Hall effect, Nature **622**, 74 (2023).

[16] B. Heinz, T. Brächer, M. Schneider, Q. Wang, B. Lägel, A. M. Friedel, D. Breitbach, S. Steinert, T. Meyer, M. Kewenig, *et al.*, Propagation of spin-wave packets in individual nanosized yttrium iron garnet magnonic conduits, Nano Lett. **20**, 4220 (2020).

[17] L. J. Cornelissen, J. Liu, R. A. Duine, J. B. Youssef, and B. J. van Wees, Long-distance transport of magnon spin information in a magnetic insulator at room temperature, Nat. Phys. **11**, 1022 (2015).

[18] K. Wang, X. Xu, Y. Cheng, M. Zhang, J.-S. Wang, H. Wang, and G. Zhang, Magnon relaxation time in ferromagnetic $Cr_2Ge_2Te_6$ monolayer governed by magnon-phonon interaction, Appl. Phys. Lett. **118**, 023102 (2021).

[19] K. Wang, J. He, M. Zhang, H. Wang, and G. Zhang, Magnon–phonon interaction in antiferromagnetic two-dimensional MXenes, Nanotechnology **31**, 435705 (2020).

[20] B. Huang, G. Clark, E. Navarro-Moratalla, D. R. Klein, R. Cheng, K. L. Seyler, D. Zhong, E. Schmidgall, M. A. McGuire, D. H. Cobden, *et al.*, Layer-dependent ferromagnetism in a van der Waals crystal down to the monolayer limit, Nature **546**, 270 (2017).

[21] C. Gong, L. Li, Z. Li, H. Ji, A. Stern, Y. Xia, T. Cao, W. Bao, C. Wang, Y. Wang, *et al.*, Discovery of intrinsic ferromagnetism in two-dimensional van der Waals crystals, Nature **546**, 265 (2017).

[22] A. F. May, D. Ovchinnikov, Q. Zheng, R. Hermann, S. Calder, B. Huang, Z. Fei, Y. Liu, X. Xu, and M. A.

McGuire, Ferromagnetism near room temperature in the cleavable van der Waals crystal Fe_5GeTe_2, ACS Nano **13**, 4436 (2019).

[23] G. Long, H. Henck, M. Gibertini, D. Dumcenco, Z. Wang, T. Taniguchi, K. Watanabe, E. Giannini, and A. F. Morpurgo, Persistence of magnetism in atomically thin $MnPS_3$ crystals, Nano Lett. **20**, 2452 (2020).

[24] Z. Fei, B. Huang, P. Malinowski, W. Wang, T. Song, J. Sanchez, W. Yao, D. Xiao, X. Zhu, A. F. May, *et al.*, Two-dimensional itinerant ferromagnetism in atomically thin Fe_3GeTe_2, Nat. Mater. **17**, 778 (2018).

[25] X. Zhang, Q. Lu, W. Liu, W. Niu, J. Sun, J. Cook, M. Vaninger, P. F. Miceli, D. J. Singh, S.-W. Lian, *et al.*, Room-temperature intrinsic ferromagnetism in epitaxial $CrTe_2$ ultrathin films, Nat. Commun. **12**, 2492 (2021).

[26] Y. Deng, Y. Yu, M. Z. Shi, Z. Guo, Z. Xu, J. Wang, X. H. Chen, and Y. Zhang, Quantum anomalous Hall effect in intrinsic magnetic topological insulator $MnBi_2Te_4$, Science **367**, 895 (2020).

[27] J. Li, Y. Li, S. Du, Z. Wang, B.-L. Gu, S.-C. Zhang, K. He, W. Duan, and Y. Xu, Intrinsic magnetic topological insulators in van der Waals layered $MnBi_2Te_4$-family materials, Sci. Adv. **5**, eaaw5685 (2019).

[28] M. A. Islam, P. Serles, B. Kumral, P. G. Demingos, T. Qureshi, A. Meiyazhagan, A. B. Puthirath, M. S. B. Abdullah, S. R. Faysal, P. M. Ajayan, *et al.*, Exfoliation mechanisms of 2D materials and their applications, Appl. Phys. Rev. **9**, 041301 (2022).

[29] G. Deokar, J. Jin, U. Schwingenschlögl, and P. M. F. J. Costa, Chemical vapor deposition-grown nitrogen-doped graphene's synthesis, characterization and applications, NPJ 2D Mater. Appl. **6**, 14 (2022).

[30] D. H. Kiem, M. Y. Jeong, H. Yoon, and M. J. Han, Strain engineering and the hidden role of magnetism in monolayer VTe_2, Nanoscale **14**, 10009 (2022).

[31] B. Tai, W. Wu, X. Feng, Y. Jiao, J. Zhao, Y. Lu, X.-L. Sheng, and S. A. Yang, Two-dimensional CoSe structures: Intrinsic magnetism, strain-tunable anisotropic valleys, magnetic Weyl point, and antiferromagnetic metal state, Phys. Rev. B **102**, 224422 (2020).

[32] X. Hu, Y. Zhao, X. Shen, A. V. Krasheninnikov, Z. Chen, and L. Sun, Enhanced ferromagnetism and tunable magnetism in Fe_3GeTe_2 monolayer by strain engineering, ACS Appl. Mater. Interfaces **12**, 26367 (2020).

[33] S. Yang, Y. Chen, and C. Jiang, Strain engineering of two-dimensional materials: Methods, properties, and applications, InfoMat **3**, 397 (2021).

[34] A. Bafekry, C. Stampfl, M. Ghergherehchi, and S. Farjami Shayesteh, A first-principles study of the effects of atom impurities, defects, strain, electric field and layer thickness on the electronic and magnetic properties of the C_2N nanosheet, Carbon **157**, 371 (2020).

[35] L. Liu, X. Hu, Y. Wang, A. V. Krasheninnikov, Z. Chen, and L. Sun, Tunable electronic properties and enhanced ferromagnetism in $Cr_2Ge_2Te_6$ monolayer by strain engineering, Nanotechnology **32**, 485408 (2021).

[36] L. Webster and J.-A. Yan, Strain-tunable magnetic anisotropy in monolayer $CrCl_3$, CrB_3, and CrI_3, Phys. Rev. B **98**, 144411 (2018).

[37] J. L. Lado and J. Fernández-Rossier, On the origin of magnetic anisotropy in two dimensional CrI_3, 2D Mater. **4**, 035002 (2017).

[38] Y. Fang, S. Wu, Z.-Z. Zhu, and G.-Y. Guo, Large magneto-optical effects and magnetic anisotropy energy in two-dimensional $Cr_2Ge_2Te_6$, Phys. Rev. B **98**, 125416 (2018).

[39] C. Xu, J. Feng, H. Xiang, and L. Bellaiche, Interplay between Kitaev interaction and single ion anisotropy in ferromagnetic CrI_3 and $CrGeTe_3$ monolayers, NPJ Comput. Mater. **4**, 57 (2018).

[40] M. Rassekh, J. He, S. Farjami Shayesteh, and J. J. Palacios, Remarkably enhanced Curie temperature in monolayer CrI_3 by hydrogen and oxygen adsorption: A first-principles calculations, Comput. Mater. Sci. **183**, 109820 (2020).

[41] M. Gibertini, M. Koperski, A. F. Morpurgo, and K. S. Novoselov, Magnetic 2D materials and heterostructures, Nat. Nanotechnol. **14**, 408 (2019).

[42] F. Reif, *Fundamentals of Statistical and Thermal Physics* (Waveland Press, Long Grove, Illinois, 2009).

[43] G. Kresse and J. Furthmüller, Efficient iterative schemes for ab initio total-energy calculations using a plane-wave basis set, Phys. Rev. B **54**, 11169 (1996).

[44] G. Kresse and J. Furthmüller, Efficiency of *ab-initio* total energy calculations for metals and semiconductors using a plane-wave basis set, Comput. Mater. Sci. **6**, 15 (1996).

[45] J. P. Perdew, K. Burke, and M. Ernzerhof, Generalized gradient approximation made simple, Phys. Rev. Lett. **77**, 3865 (1996).

[46] G. Kresse and J. Hafner, *Ab initio* simulation of the metal/nonmetal transition in expanded fluid mercury, Phys. Rev. B **55**, 7539 (1997).

[47] S. L. Dudarev, G. A. Botton, S. Y. Savrasov, C. J. Humphreys, and A. P. Sutton, Electron-energy-loss spectra and the structural stability of nickel oxide: An LSDA + U study, Phys. Rev. B **57**, 1505 (1998).

[48] A. Georges and G. Kotliar, Hubbard model in infinite dimensions, Phys. Rev. B **45**, 6479 (1992).

[49] S. Kang, S. Kang, and J. Yu, Effect of Coulomb interactions on the electronic and magnetic properties of two-dimensional $CrSiTe_3$ and $CrGeTe_3$ materials, J. Electron. Mater. **48**, 1441 (2019).

[50] L. Liu, X. Ren, J. Xie, B. Cheng, W. Liu, T. An, H. Qin, and J. Hu, Magnetic switches via electric field in BN nanoribbons, Appl. Surf. Sci. **480**, 300 (2019).

[51] Z. Wu, Z. Shen, Y. Xue, and C. Song, Strain-induced topological phase transition and enhanced Curie temperature in $MnBi_2Te_4/CrI_3$ heterojunction, Phys. Rev. Mater. **6**, 014011 (2022).

[52] S.-D. Guo, J.-X. Zhu, M.-Y. Yin, and B.-G. Liu, Substantial electronic correlation effects on the electronic properties in a Janus FeClF monolayer, Phys. Rev. B **105**, 104416 (2022).

[53] S.-D. Guo, X.-S. Guo, Y.-T. Zhu, and Y.-S. Ang, Predicted ferromagnetic monolayer CrSCl with large vertical piezoelectric response: A first-principles study, Appl. Phys. Lett. **121**, 062403 (2022).

[54] C. Tang, K. Ostrikov, S. Sanvito, and A. Du, Prediction of room-temperature ferromagnetism and large perpendicular magnetic anisotropy in a planar hypercoordinate FeB_3 monolayer, Nanoscale Horiz. **6**, 43 (2021).

[55] X. Gonze, Adiabatic density-functional perturbation theory, Phys. Rev. A **52**, 1096 (1995).

[56] See the Supplemental Material at http://link.aps.org/supplemental/10.1103/PhysRevApplied.21.054036 for four possible magnetic configurations, the contribution of magnetic anisotropy to the magnon Hamiltonian and Curie temperature, the spin-wave spectrum based on the Heisenberg model, phonon dispersion, the stress-strain relationship and stiffness tensor of the $CrGeTe_3$ monolayer, contributions from the dynamic magnon-magnon interaction to the magnon frequency, spin autocorrelation functions, and the magnetic moment per Cr^{3+} ion versus magnetic field of the pristine $CrGeTe_3$ monolayer.

[57] H. Xiang, C. Lee, H.-J. Koo, X. Gong, and M.-H. Whangbo, Magnetic properties and energy-mapping analysis, Dalton Trans. **42**, 823 (2013).

[58] H. J. Xiang, E. J. Kan, S.-H. Wei, M. H. Whangbo, and X. G. Gong, Predicting the spin-lattice order of frustrated systems from first principles, Phys. Rev. B **84**, 224429 (2011).

[59] S. Streib, N. Vidal-Silva, K. Shen, and G. E. W. Bauer, Magnon-phonon interactions in magnetic insulators, Phys. Rev. B **99**, 184442 (2019).

[60] L. Chen, C. Mao, J.-H. Chung, M. B. Stone, A. I. Kolesnikov, X. Wang, N. Murai, B. Gao, O. Delaire, and P. Dai, Anisotropic magnon damping by zero-temperature quantum fluctuations in ferromagnetic $CrGeTe_3$, Nat. Commun. **13**, 4037 (2022).

[61] K. Wang, X. Xu, Y. Cheng, M. Zhang, J.-S. Wang, H. Wang, and G. Zhang, Magnon-magnon interaction and magnon relaxation time in a ferromagnetic $Cr_2Ge_2Te_6$ monolayer, Phys. Rev. B **102**, 235434 (2020).

[62] L. R. Mead and N. Papanicolaou, Holstein-Primakoff theory for many-body systems, Phys. Rev. B **28**, 1633 (1983).

[63] M. M. Nieto and D. R. Truax, Holstein-Primakoff/Bogoliubov transformations and the multiboson system, Fortschr. Phys. **45**, 145 (1997).

[64] G.-C. Wick, The evaluation of the collision matrix, Phys. Rev. **80**, 268 (1950).

[65] S. Halilov, A. Perlov, P. Oppeneer, and H. Eschrig, Magnon spectrum and related finite-temperature magnetic properties: A first-principle approach, Europhys. Lett. **39**, 91 (1997).

[66] S. Halilov, H. Eschrig, A. Y. Perlov, and P. Oppeneer, Adiabatic spin dynamics from spin-density-functional theory: application to Fe, Co, and Ni, Phys. Rev. B **58**, 293 (1998).

[67] B. H. Zhang, Y. S. Hou, Z. Wang, and R. Q. Wu, First-principles studies of spin-phonon coupling in monolayer $Cr_2Ge_2Te_6$, Phys. Rev. B **100**, 224427 (2019).

[68] K. Wang, K. Ren, Y. Cheng, M. Zhang, H. Wang, and G. Zhang, Effects of molecular adsorption on the spin-wave spectrum and magnon relaxation in two-dimensional $Cr_2Ge_2Te_6$, Phys. Chem. Chem. Phys. **22**, 22047 (2020).

[69] F. Mouhat and F.-X. Coudert, Necessary and sufficient elastic stability conditions in various crystal systems, Phys. Rev. B **90**, 224104 (2014).

[70] V. Wang, G. Tang, R.-T. Wang, Y.-C. Liu, H. Mizuseki, Y. Kawazoe, J. Nara, and W.-T. Geng, High-throughput computational screening of two-dimensional semiconductors, arXiv preprint arXiv:1806.04285 (2018).

[71] Y. Yin, D. Li, Y. Hu, G. Ding, H. Zhou, and G. Zhang, Phonon stability and phonon transport of graphene-like borophene, Nanotechnology **31**, 315709 (2020).

[72] X. Chen, J. Qi, and D. Shi, Strain-engineering of magnetic coupling in two-dimensional magnetic semiconductor $CrSiTe_3$: Competition of direct exchange interaction and superexchange interaction, Phys. Lett. A **379**, 60 (2015).

[73] Y. Hou, Y. Wei, D. Yang, K. Wang, K. Ren, and G. Zhang, Enhancing the Curie temperature in $Cr_2Ge_2Te_6$ via charge doping: A first-principles study, Molecules **28**, 3893 (2023).

[74] J. Kanamori, Superexchange interaction and symmetry properties of electron orbitals, J. Phys. Chem. Solids **10**, 87 (1959).

[75] J. B. Goodenough, Theory of the role of covalence in the perovskite-type manganites [La, M(II)] MnO_3, Phys. Rev. **100**, 564 (1955).

[76] L. Passell, O. W. Dietrich, and J. Als-Nielsen, Neutron scattering from the Heisenberg ferromagnets EuO and EuS. I. The exchange interactions, Phys. Rev. B **14**, 4897 (1976).